

Nanoscale

Accepted Manuscript



This is an *Accepted Manuscript*, which has been through the Royal Society of Chemistry peer review process and has been accepted for publication.

Accepted Manuscripts are published online shortly after acceptance, before technical editing, formatting and proof reading. Using this free service, authors can make their results available to the community, in citable form, before we publish the edited article. We will replace this *Accepted Manuscript* with the edited and formatted *Advance Article* as soon as it is available.

You can find more information about *Accepted Manuscripts* in the [Information for Authors](#).

Please note that technical editing may introduce minor changes to the text and/or graphics, which may alter content. The journal's standard [Terms & Conditions](#) and the [Ethical guidelines](#) still apply. In no event shall the Royal Society of Chemistry be held responsible for any errors or omissions in this *Accepted Manuscript* or any consequences arising from the use of any information it contains.



Nanoscale

PAPER

Interactions between C and Cu atoms in single-layer graphene: direct observation and modelling†

Received 00th January 20xx,
Accepted 00th January 20xx

DOI: 10.1039/x0xx00000x

www.rsc.org/

Emi Kano,^{*ab} Ayako Hashimoto,^{abcd} Tomoaki Kaneko,^e Nobuo Tajima,^e Takahisa Ohno,^e and Masaki Takeguchi^{abc}

Metal doping into the graphene lattice has been studied recently to develop novel nanoelectronic devices and to gain understanding of the catalytic activities of metals in nanocarbon structures. Here we report direct observation of interactions between Cu atoms and single-layer graphene by transmission electron microscopy. We document stable configurations of Cu atoms in the graphene sheet and unique transformations of graphene promoted by Cu atoms. First-principles calculations based on density functional theory reveal a reduction of energy barrier that caused rotation of C-C bonds near Cu atoms. We discuss two driving forces, electron irradiation and *in situ* heating, and conclude that the observed transformations were mainly promoted by electron irradiation. Our results suggest that individual Cu atoms can promote reconstruction of single-layer graphene.

Introduction

Interactions between metals and graphene have been extensively studied aiming to control the local properties of graphene for applications in electrocatalysts and nanoelectronic devices^{1–3} and to create novel carbon nanostructures.^{4–7} Theoreticians predicted that transition metal atoms in graphene vacancies have unique electronic and magnetic properties.^{8–10} However, there are only a few experimental reports on such metal–graphene systems, due to the difficulty of their direct observation. Researchers applied aberration-corrected transmission electron microscopy (TEM) and scanning TEM (STEM) to observe metal atoms in a graphene sheet, such as Fe dimers¹ and single atoms of Pt, Co and In¹¹ doped into graphene vacancies, as well as etching of graphene mediated by metal atoms (Cr, Ti, Pd, Ni or Al).¹² These studies suggest that most metal atoms, except for Au, promote etching of graphene. Such destruction of graphene will result in a serious problem for practical applications.

Here we report the structures and dynamics of Cu atoms embedded in a single-layer graphene observed by aberration-corrected TEM. We selected Cu because it has a similar

electronic configuration to Au and is known to be the best catalyst for graphene growth^{13–15}; hence, Cu will not etch graphene and is expected to catalyse the growth or modification of graphene structures. We directly observed unique morphological changes in Cu-doped graphene that have not been observed with other metals: reconstruction of graphene grains, various transformations promoted near Cu atoms, and formation and mending of nanopores. First-principles calculations based on density functional theory (DFT) were performed to explain the observed stability and dynamics, as well as Cu-assisted transformations of graphene.

Results and discussion

Cu sites in graphene

In the areas irradiated by focused electron beam, some Cu atoms replaced carbon atoms in the graphene lattice. This substitution was observed more frequently in areas containing residual oxygen and hydrocarbon contaminations. These contaminations could be reduced by *in situ* annealing. Thus the density of Cu-C substitutions in graphene could be controlled by electron beam current and sample annealing temperature, which may be useful for practical applications.

The TEM image of Fig. 1a shows more than 10 Cu atoms embedded in a $\sim 4 \times 4$ nm² area of graphene. We took TEM images at overfocus conditions to highlight Cu atoms, and Cu atoms appeared 1.8 ± 0.2 times brighter than C atoms. Meanwhile, at underfocus (Scherzer focus) the contrasts are reversed and Cu atoms are more difficult to image. Multislice simulation for the present overfocus conditions yielded a Cu/C intensity ratio of 1.92 (further details on Cu identification are given in Supplementary Figs. S1–3).

^a Graduate School of Pure and Applied Sciences, University of Tsukuba, Tsukuba, 305-8573, Japan. E-mail: KANOU.Emi@nims.go.jp

^b Surface Physics and Structure Unit, National Institute for Materials Science, Tsukuba, 305-0047, Japan.

^c Transmission Electron Microscopy Station, National Institute for Materials Science, Tsukuba, 305-0044, Japan.

^d Global Research Center for Environment and Energy based on Nanomaterials Science, National Institute for Materials Science, Tsukuba, 305-0047, Japan.

^e Computational Materials Science Unit, National Institute for Materials Science, Tsukuba, 305-0044, Japan.

† Electronic Supplementary Information (ESI) available: Three TEM movies, additional TEM data corresponding to movies, calculated models, and lifetime results. See DOI: 10.1039/x0xx00000x

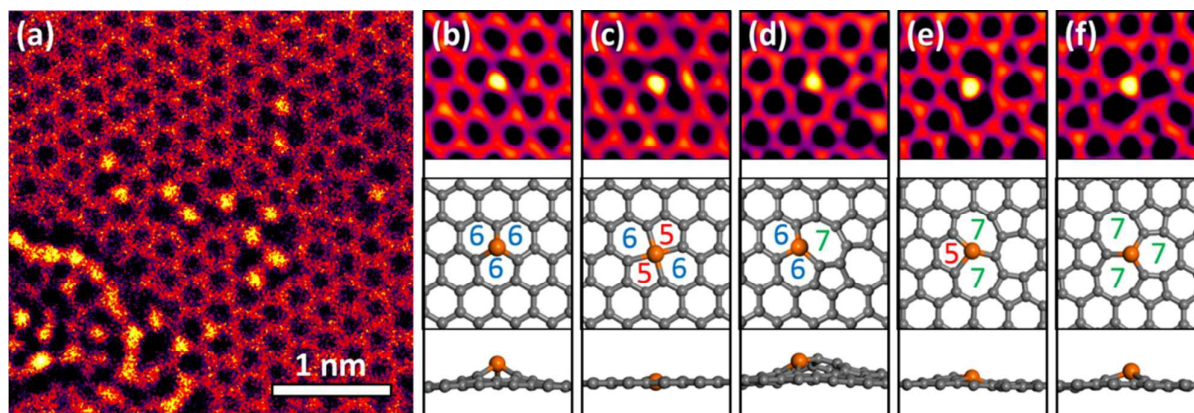


Figure 1 Cu atoms embedded in graphene. (a) Unprocessed TEM image of Cu atoms (brighter spots) embedded in graphene. (b–f) Averaged and low-pass-filtered TEM images (top row) and corresponding DFT models of Cu sites (top and side views, second and third rows, respectively).

Most of previous studies^{1, 8–11, 16} focused on metal atoms in single or double vacancies (Figs. 1b, and c), i.e., the cases when metal atoms substituted for one or two carbon atoms in a pristine graphene lattice. In contrast, the Cu atoms in our experiments exhibited a more complex behaviour and were frequently observed at topological defects in graphene (Figs. 1d–f). We name the corresponding structures according to the number of atoms making up the carbon rings, including the central Cu atom. For example, the Cu atom shown in Fig. 1d makes two six-membered rings and one seven-membered ring with neighbouring C atoms, so we call this structure 667.

DFT calculations suggest that most Cu-related defects are not planar, except for those containing four-coordinated Cu (Fig. 1c). Three-coordinated Cu atoms (Figs. 1b and d–f) protrude from the graphene surface because single vacancies are too small to accommodate them. The height is the smallest for the 577 structure shown in Fig. 1e, whereas in the 667 configuration several carbon atoms are displaced out of graphene plane along with Cu. Malola *et al.*¹⁶ claimed that Au preferentially occupies double or larger vacancies to reduce the height; however, we observe no clear correlation between the height and stability (lifetime) of the observed structures. For example, the highly distorted 667 was more frequently observed and had a longer lifetime than the almost planar 577 structure. Krashennnikov *et al.*⁹ found that metal atoms, including Cu and Au, form covalent bonds with the C atoms at the vacancies. The stability primarily depends on the strain around the Cu atoms and the bonding strength between Cu and C; hence, the height of a defect is not a decisive factor.

In addition, Cu atoms physically adsorbed on a pristine graphene surface were rarely observed, because their diffusion barrier is more than 10 times lower than that of substitutional Cu atoms.¹⁷ The energy provided by heating and electron irradiation was sufficient to transform Cu atoms embedded in graphene and was too large to observe atoms adsorbed on its surface.

Reconstruction of graphene

Cu substitution resulted in a gradual reconstruction of graphene during the TEM observations. Figure 2a was taken 13 min after Fig. 1a from the same sample area. A small misoriented region was created near Cu atoms. It contains pairs of five- and seven-membered rings at a 30° grain boundary (yellow in Fig. 2b). Such pairs are called Stone–Wales (SW) defects. Figures 2c and d show TEM images taken before and after the reconstruction taken from another area. Note the broadening of the corresponding Fast Fourier transform (FFT) patterns (cf. insets in Figs. 2c and d), which reveals that the reconstruction resulted in an angular disorder due to the formation of 1–3 nm sized grains. We numbered the four grains shown in Fig. 2d as follows: grain #1 kept its original orientation, but became a bit distorted; #2 and #4 reconstructed and rotated by 18° and 23° from the original, respectively; and #3 rotated while preserving its original six-membered ring structure.

Most grains were disrupted by the local strain induced by the contaminants and reconstructed via repeated rotation of C–C bonds near Cu atoms to minimize the overall strain. In Fig. 2a, hydrocarbon contaminants on the left side of the image were partially graphitized by electron irradiation, distorting the underlying graphene lattice. Grain #2 was also covered by hydrocarbons (Fig. 2c); it reconstructed after their removal by electron irradiation, albeit with a different orientation.

Supplementary Movie S1 was taken 15–21 min after Fig. 2c, which shows a different type of reconstruction, namely a grain rotation. In contrast to the former reconstruction, the grains kept the original graphene structure during the reconstruction. Grain #3 retained its orientation until a small pore was mended by Cu atoms, and gradually rotated by about 17° owing to the strain from contaminants on the left and defects on the right side (see Supplementary Fig. S4). During this process, many SW defects moved via C–C bond rotation and helped fit grain #3 to its neighbours.

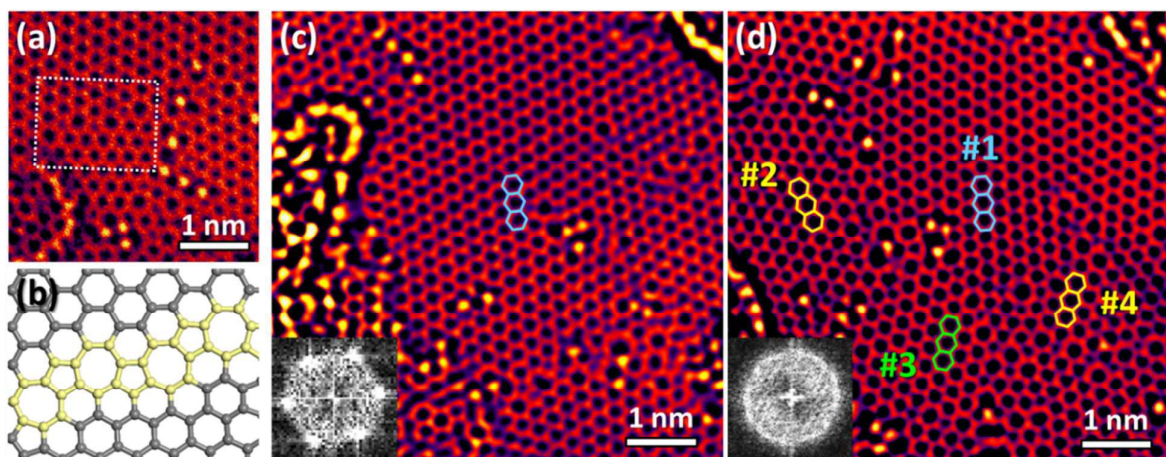


Figure 2 Reconstruction of graphene. (a) TEM image taken after ~13 min from the same area as shown in Fig. 1a. (b) Model of grain boundary marked by the white box in (a). Five- and seven-membered rings appear in yellow. (c) TEM image taken before the reconstruction. (d) TEM image taken 20 min after (c). Insets in (c) and (d) are FFT images.

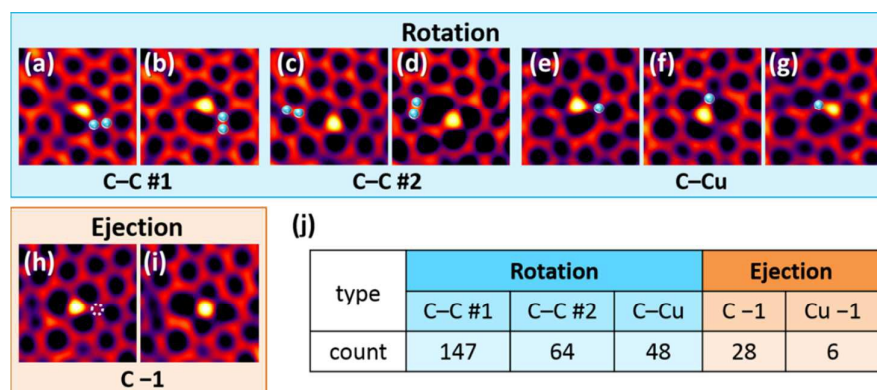


Figure 3 TEM images of the structures before and after each transformation: (a, b) rotation of C-C bond attached to a Cu atom, (c, d) rotation of C-C bond near a Cu atom, (e-g) rotation of C-Cu bond, and (h, i) ejection of C atom next to Cu. Rotated C atoms are highlighted as light blue balls. (j) Observation frequency for each transformation (arb. units).

Lehtinen *et al.*¹⁸ found that aggregated interstitials in graphene, which have a strong local curvature in graphene, are energetically more favourable than isolated ones. The same was true of Cu atoms and SW defects: SW defects were reported to distort graphene,¹⁹⁻²⁰ and Cu atoms in our experiment tended to combine with them rather than remain isolated. Cu atoms can also distort graphene, thereby promoting both generation of defects and their healing via C-C bond rotation. Such repeated distortion and reconstruction, promoted by Cu atoms and electron irradiation, gradually changed the graphene structure.

Transformations promoted by Cu atoms

We analysed the dynamics and stability of 56 single Cu atoms to further elaborate the graphene transformations mentioned above. Figure 3 shows the four typical transformation types: (a-b) and (c-d) are C-C bond rotations #1 and #2. They differ by that in #1 one of the rotating C atoms is attached to a Cu

atom, while in #2 the rotating pair is separated from Cu. The third transformation is rotation of a C-Cu bond (e-g), and the fourth is ejection of one C atom (h-i). Selected images were converted into an animation which includes all transformation types (see Supplementary Movie S2 and Fig. S5).

The majority of the observed transformations were C-C rotations near the Cu atoms. C-C rotation #1 was most common and occurred reversibly, while C-C rotation #2 was less frequent (Fig. 3j). We can explain this preference by the number of bonds that break and recombine during each transformation. Two strong C-C bonds break in process #2, whereas #1 involves one C-C bond and one weak C-Cu bond. The binding energies of substitutional C and Cu atoms in graphene were calculated as 15.7 and 3.9 eV, respectively. Because each C and Cu atom is bonded with three neighbouring C atoms, the energy difference between one C-C bond and one C-Cu bond, or between rotations #2 and #1, is estimated to be ~4 eV. This scenario explains the relative

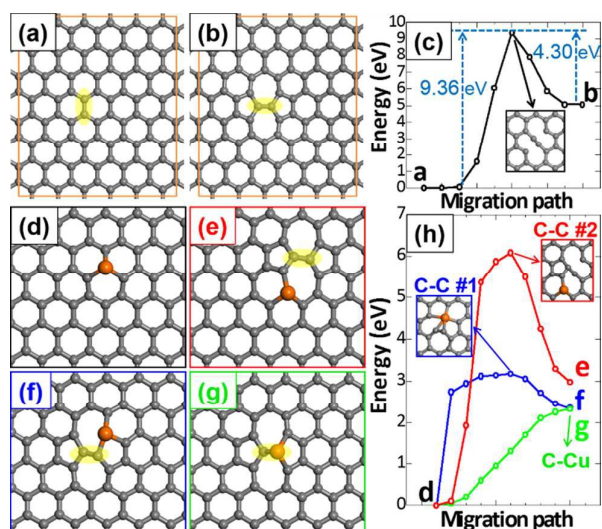


Figure 4 Energy required for the bond rotations. (a, b) Atomic models of C–C bond rotation without Cu atoms. Orange frames outline the cells used in DFT calculation, which contain 96 atoms. (c) Energy diagram of transformation between (a) and (b). (d–g) Atomic models of Cu sites in graphene. If the two carbon atoms highlighted by yellow ellipses are rotated, the model of Cu atoms embedded in SW defects (e–g) will become pristine structure (d). (h) Energy diagrams of transformations between (d) and (e), (f) and (g). Insets show models of transition states.

frequencies of C–C rotations #1 and #2, but not of the other transformations: it predicts that C–C #1 and C–Cu rotation should be equally frequent, as they both involve one C–C and one C–Cu bond. Meanwhile the C–C #1 process was 3 times more common in our observations. Furthermore, C ejections were rather common, despite their expected high energy barrier, whereas very few Cu ejections were observed. We discuss this inconsistency later.

We performed first-principles calculations based on DFT, to evaluate the activation energy barrier and the total energy change for each transformation. Our DFT calculations of the energy barrier do explain why the C–C rotations are promoted by Cu atoms. They agree with the analysed observation frequency (Fig. 3j) and stability (lifetime) of each structure and the binding energy estimates mentioned above, although they are simplified models and do not take in account the defect-related lattice distortions in the large area.

Figures 4a and b show the C–C rotation that converts four six-membered rings into two SW defects. Replacing one C atom with a Cu atom in these figures results in the 666, 667, 567 and 577 defects as shown in Figs. 4d–g, respectively (see Supplementary Fig. S6 for other Cu configurations). Figure 4c shows the energy diagram of C–C bond rotation *without* Cu atom. The total energy increased by 5.06 eV when a SW defect was created. The top of the barrier corresponds to the transition state with two broken C–C bonds; it is 9.36 eV above the pristine graphene and 4.30 eV above the SW defect level. These values are consistent with a previous report²¹. As

discussed below, the 9.36 eV energy can be easily supplied by a typical TEM operated at 200–300 kV, but not at 80 kV.

We also calculated C–C bond rotation *with* Cu atoms (Figs. 4d–f), and found that the energy barrier of C–C rotations was significantly reduced from that in pristine graphene (Fig. 4h). The C–C rotation #1 was most frequently observed, because the energy barrier was reduced to 3.18 eV, and the energy required to return to the 666 structure in Fig. 4d was only 0.84 eV. This reduction came from the low C–Cu binding energy and from the partial passivation of carbon dangling bonds by Cu (see inset in Fig. 4h).

The stability of each structure depends on the energy barrier height rather than the total energy difference. For example, although the SW defect is 5.06 eV less stable than pristine graphene, once it is created, the energy barrier of 4.30 eV prevents its relaxation from SW defect to pristine graphene. The 577 structure (Fig. 4g) has a lower total energy than the 667 structure (Fig. 4e); however, there is no transition state between the 577 structure and the 666 structure (Fig. 4d), as shown in Fig. 4h; therefore, it will soon transform into 666 (the pristine structure without SW defects). Cu atom at the vertex of the pentagon induces a large stress in graphene and therefore is less stable than in the other configurations, despite the low total energy of its optimized structure.

This factor appears in our experimental observations as the defect lifetime. Defects involving five-membered rings, such as 577 and 568, had approximately half the lifetime of the 667 or 677 structures (see Supplementary Table S1). The 577 structure can also be regarded as a transition state of diffusion of Cu atom. The Cu atom in the 666 structure will exchange positions with the neighbouring C atom by the 180° C–Cu rotation. The corresponding energy barrier is 2.32 eV (energy difference between the 577 and 666 states), which is similar to the value of 2.2 eV for Au atom diffusion in graphene.²²

Driving force of the transformations

In this section, we discuss two driving forces: *in situ* heating and electron irradiation. C–C bond rotations occurred within 5 min in our experiment, which had a temporal resolution of 1 s. We estimated the energy required to rotate the C–C bond at 3.2 eV, which is sufficient to cause SW defect formation by C–C rotation #1 and relaxation by C–C rotation #2, as shown in Fig. 4h. We then calculated the time required for the next rotation via thermal activation²³: the C–C bond rotation takes $\sim 10^{15}$ s at 300 °C, with an attempt frequency of 5×10^{12} s⁻¹ given by the G-mode vibration of graphene.²⁴ This calculation suggests that most transformations could not be induced by thermal activation (except for the relaxation of SW defects via C–C rotation #1), and were promoted by electron irradiation. This conclusion is supported by our observations that graphene structure remained unchanged in weakly irradiated sample areas.

When an electron is elastically scattered at an angle θ by an atom, it transforms an energy E_i to it^{25} ; E_i increases with θ and decreases with the atomic mass number (12 and 63.5 for C and Cu, respectively). We used an accelerating voltage of 80 kV because the corresponding E_i value is lower than the

sputtering threshold energy (~ 22 eV^{26–27}), which reduces the knock-on damage. However, this low beam energy can still induce transformations in Cu-doped graphene, with carbon atoms being more susceptible owing to their low atomic number. The maximum transfer energies E_{\max} (E_t at $\theta = 180^\circ$) are 15.74 eV for C and 2.97 eV for Cu.

The energy transfer model can explain why C–C bond rotation and C atom ejection were more frequently observed than C–Cu bond rotation and Cu ejection. The energy transferred to Cu atoms cannot exceed 2.97 eV; hence, the observed transformations arose mainly via excitation of C atoms. Electron irradiation has less effect on Cu; thus, Cu atoms moved less than C atoms. Although the binding energy of a Cu atom in a single vacancy is 4–5 times smaller than that of a C atom, Cu atom ejections from the graphene lattice were rarely observed in our TEM experiments. The ejected C and Cu atoms likely moved too fast to be observed by TEM and were trapped by other vacancies or contaminants in graphene. Cu atoms are expected to be more mobile near contaminants or nanoparticles than in a perfect graphene lattice.

For all the transformations described above, the energy transferred from electron beams should be greater than the energy barrier E_b . The scattering cross section σ for an energy transfer $E_t \geq E_b$ is given by,^{23, 25}

$$\begin{aligned} \sigma(\theta_{\min}) &= 2\pi \int_{\theta_{\min}}^{\pi} \frac{d\sigma_{\text{el}}}{d\Omega} \sin\theta d\theta \\ &= \frac{4Z^2 R^4 (1 + E_t/E_0)^2}{a_H^2} 2\pi \int_{\theta_{\min}}^{\pi} \frac{\sin\theta}{[1 + (\theta + \theta_0)^2]^2} d\theta \end{aligned}$$

$$\text{with } R = a_H Z^{-1/3}, \theta_0 = \lambda/2\pi R$$

where θ_{\min} is the minimum scattering angle given by equation $E_t = E_{\max} \sin^2(\theta/2)$, $d\sigma_{\text{el}}/d\Omega$ is the differential elastic cross section, a_H is the Bohr radius (5.29×10^{-11} m), Z is the atomic number (6 for C and 29 for Cu), and E_0 is the electron rest energy (0.511 MeV). Thus, taking $E_b = 3.2$ eV for C–C rotation (which leads to $\theta_{\min} = 54^\circ$ for carbon), we obtain $\sigma = 2.9 \times 10^{-6}$ Å. The defect lifetime t is inversely proportional to the product of σ and electron beam current density j ($t = 1/\sigma j$).

Figure 5 shows the averaged lifetimes, including all types of structures and transformations, at different current densities (respective lifetime values of typical structures are shown in Supplementary Table S1). The green and blue symbols respectively show the experimental values measured at 150 °C and the calculated values, assuming the energy transferred to C is 7.26 eV (the maximum value for C–C bond rotation near a Cu atom). Although the experimental lifetimes are slightly longer than the calculated ones, their orders of magnitude are the same, and both lifetimes are inversely proportional to current density j . For $j = 125$ A/cm² at 150 °C, transformations occurred within a few seconds in defective areas, whereas stable structures such as 667, 666, 677 and 5656 in a relatively clean graphene often survived for more than 2 min. We conclude that Cu atoms promote C–C rotation when they are

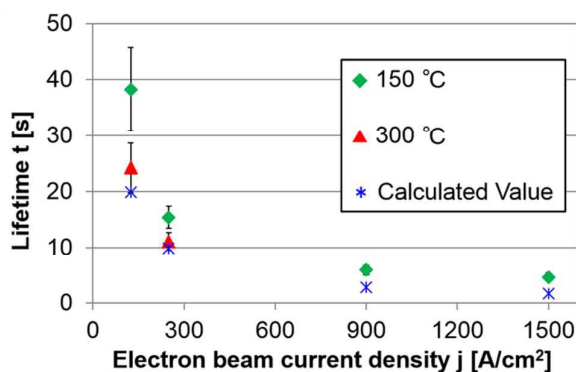


Figure 5 Lifetime under electron irradiation. Observed lifetimes at 150 and 300 °C were averaged and plotted as a function of the electron beam current density. Blue symbols indicate the calculated values assuming that $E_t = 7.26$ eV for C.

surrounded by many defects, but not when reconstruction of the graphene is complete.

As shown in Fig. 5, the temperature effect on the lifetime t became significant at lower current density j , although it was smaller than the electron irradiation effect. In contrast to the energy transferred from electron beam, the thermal activation energy affects C and Cu equally; hence, increasing the temperature reduced the lifetime of every Cu-graphene configuration. Gan *et al.*²⁸ measured the diffusion rates of Pt and Au atoms at different temperatures and calculated the diffusion barriers. However, Malola *et al.*¹⁶ pointed that these results may not be accurate because of the strong irradiation effect. Further observations are necessary for a quantitative discussion of the temperature effect, especially at low electron beam densities (≤ 125 A/cm²).

Cu atoms and nanoparticles started to evaporate at much lower temperature than the melting temperature 1085 °C of bulk Cu. Electron irradiation also promoted the aggregation and evaporation of Cu; however, Cu nanoparticles were evaporated only by heating. We took a low-magnification TEM image (Supplementary Fig. S1c) and then turned off the beam. About half of the nanoparticles have disappeared after 11 h of heating at 300 °C. Cu atoms embedded in the graphene lattice were more stable than the particles physically adsorbed on the graphene surface. The ejection frequency of Cu atoms from the graphene lattice did not increase at 300 °C compared to that at 150 °C. However, above 300 °C, Cu evaporated very rapidly, before promoting Cu substitutions. Such heating should be avoided when manufacturing Cu-doped graphene devices.

Uniqueness of Cu compared with other transition metals

Many metals, including Cr, Ti, Pd, Ni and Al, were experimentally reported to etch graphene,¹² and a similar activity was theoretically predicted for Fe and Co.²⁹ Cu atoms, however, promoted graphene reconstruction rather than etching in our experiment. Even when small pores were created by irradiation, Cu atoms covered their edges to prevent

expansion of the pores and mended them by trapping C atoms floating around (e.g. Supplementary Fig. S4b). We have not observed such effects for Pt under similar experimental conditions.³⁰ Double-vacancy transformation processes were observed in graphene without Cu atoms (Supplementary Movie S3 and Fig. S7), however, they occurred at an angstrom rather than nanometre scale.

We believe this unique ability of Cu originates from its electronic configuration specific to noble metals. The binding energy of Cu at the single and double vacancy was calculated as 3.90 and 5.26 eV, respectively, whereas those of the other transition metals are 6–8 eV.^{8–9} While diffusing, these metal atoms bind C atoms and remove them from the graphene lattice. This effect should be much smaller for Cu, Ag, Au (binding energy 2–5 eV) and Zn atoms (binding energy 1–3 eV).^{8–9}

Furthermore, we also calculated the energy difference ΔE between Fe, Cr, and Ni substitutional atoms at SW defects and those at single vacancy without SW defects (models and results are shown in Supplementary Fig. S6). We found that their ΔE are ~ 1 eV higher than for the Cu atoms in the same models; hence, compared to Fe, Cr, and Ni, Cu atoms are more stable near SW defects and thereby promote C–C bond rotations and unique reconstructions.

Conclusions

We directly observed atomic-scale transformations of Cu-doped graphene by aberration-corrected TEM. Our observations suggest that Cu atoms tend to combine with SW defects and preferentially replace C atoms in defective graphene areas. They also modify graphene by promoting C–C bond rotation, formation and mending of nanopores, and rotation of grains mediated by contaminants and lattice defects. Cu atoms and SW defects form grain boundaries between the reconstructed and original grains. All these transformations were assisted by electron irradiation, which affected C atoms much more than Cu atoms because of the higher energy transferred to them from the electron beam. Thermal effects need a further study, and our results reveal that Cu atoms are stable in graphene sheets up to 300 °C. We combined experiment with DFT calculations to investigate the stability of Cu atoms embedded in graphene and the activation energy barriers for the experimentally observed transformations. Our results reveal that individual Cu atoms can catalyse reconstruction of carbon nanostructures.

Methods

Sample preparation

Single-layer graphene on a Cu foil was transferred onto *in situ* heating chips (E-chips for AduroTM, Protochips) using the previously reported poly(methyl methacrylate) support method³⁰. To avoid metallic impurities we etched the Cu foil with a metal-free (NH₄)₂S₂O₈ (ammonium persulfate) solution. Heating in a vacuum of $0.6\text{--}1 \times 10^{-5}$ Pa at high

temperatures above 400 °C created clean graphene patches about 200×200 nm² in size. Cu was then deposited using an ion beam etching system (PECS, Gatan). When observed at room temperature just after deposition, Cu had not formed crystals; it was dispersed with oxygen and hydrocarbons. A recent study suggests that partial oxidation of Cu suppresses nucleation, and a large graphene sheet with a single domain can be synthesized³¹. In fact, oxidized Cu nanoparticles promoted etching of graphene, whereas pure Cu nanoparticles did not. Therefore, we heated the sample at 150–300 °C to remove oxygen, and Cu atoms formed nanoparticles (the corresponding size distributions are shown in Supplementary Fig. S1). Cu nanoparticles gradually evaporated at 300 °C and rapidly disappeared at ~ 500 °C. Si contamination was possible because we used quartz-tube furnaces and silicon nitride *in situ* heating chips, yet we believe that Si was a minor impurity and most of observed atoms were Cu. Indeed all nanoparticles around the observation areas and a few dispersed atoms were identified as Cu by STEM combined with electron energy loss spectroscopy (EELS, Fig. S2).

TEM imaging experiments

Aberration-corrected TEM (JEM-ARM200F, JEOL) was used for *in situ* observations. The microscope was operated at a relatively low voltage of 80 kV to reduce knock-on damage to the graphene sheets. The sample temperature during observation was kept at 150 and 300 °C by an *in situ* heating holder (AduroTM, Protochips). Most results are reported for 150 °C, unless mentioned otherwise, but the frequency of each transformation type and lifetimes of each structure were measured at both temperatures. TEM movies were acquired at a speed of 0.5–2 frames/s. All the TEM images shown in Figs. 1–3, except for Fig. 1a, are snapshots from the TEM movies that are processed as follows: frames were shifted to compensate for thermal drift, and then averaged and low-pass filtered to improve the signal-to-noise ratio (Figs. 1a and 2a are unfiltered images).

First-principles calculations

We performed first-principles calculations based on DFT using the PHASE/0 code³². The generalized gradient approximation³³ and ultrasoft pseudopotential³⁴ were employed. The spin polarization was considered. The cut-off energies of the plane-wave basis set and charge density were taken at 25 and 255 Ry, respectively. Each defect was introduced in a graphene supercell of $6 \times 4\sqrt{3}$ periodicity (96 atoms). The lateral size of the unit cell was measured using the optimized lattice constant of graphene, 2.476 Å, which is 0.6% larger than the experimental lattice constant. The graphene sheet was isolated by a vacuum layer 10 Å thick (we used 12-Å-thick cells with ~ 2 Å distortion height). A Monkhorst and Pack mesh of $3 \times 3 \times 1$ size was used for k-sampling³⁵. The atomic positions were optimized until the residual force became smaller than 5.0×10^{-4} hartree/bohr. To evaluate energy barriers, a climbing image nudged elastic band method with eight images was employed³⁶.

Acknowledgements

We thank Dr. E. Okunishi from JEOL Ltd. for his help with STEM-EELS, Dr. Y.-C. Lin from AIST for his advice on sample preparation, and Dr. K. Iakoubovskii from NIMS for discussions. A part of this work was supported by the 'Nanotechnology Platform Project' sponsored by the Ministry of Education, Culture, Sports, Science and Technology (MEXT), Japan, and a Grant-in-Aid for Japan Society for the Promotion of Science (JSPS) Fellows.

Notes and references

- Z. He, K. He, A. W. Robertson, A. I. Kirkland, D. Kim, J. Ihm, E. Yoon, G.-D. Lee and J. H. Warner, *Nano Lett.*, 2014, **14**, 3766–3772.
- E. Yoo, T. Okata, T. Akita, M. Kohyama, J. Nakamura and I. Honma, *Nano Lett.*, 2009, **9**, 2255–2259.
- K. Pi, K. M. McCreary, W. Bao, W. Han, Y. F. Chiang, Y. Li, S.-W. Tsai, C. N. Lau and R. K. Kawakami, *Phys. Rev. B*, 2009, **80**, 075406.
- X. Li, W. Cai, L. Colombo and R. S. Ruoff, *Nano Lett.*, 2009, **9**, 4268–4272.
- S. Saadi, F. Abild-Pedersen, S. Helveg, J. Sehested, B. Hinnemann, C. C. Appel and J. K. Nørskov, *J. Phys. Chem. C*, 2010, **114**, 11221–11227.
- P. Han, K. Akagi, F. F. Canova, H. Mutoh, S. Shiraki, K. Iwaya, P. S. Weiss, N. Asao and T. Hitosugi, *ACS Nano*, 2014, **8**, 9181–9187.
- J.-Y. Raty, F. Gygi and G. Galli, *Phys. Rev. Lett.*, 2005, **95**, 096103.
- E. J. G. Santos, A. Ayuela and D. Sánchez-Portal, *New J. Phys.*, 2010, **12**, 053012.
- A. V. Krasheninnikov, P. O. Lehtinen, A. S. Foster, P. Pyykkö and R. M. Nieminen, *Phys. Rev. Lett.*, 2009, **102**, 126807.
- Z. Ning, Z. Chen, X. Du, R. Ran, W. Dong and C. Chen, *J. Supercond. Nov. Magn.*, 2013, **27**, 115–120.
- H. Wang, Q. Wang, Y. Cheng, K. Li, Y. Yao, Q. Zhang, C. Dong, P. Wang, U. Schwingenschlögl, W. Yang and X. X. Zhang, *Nano Lett.*, 2012, **12**, 141–144.
- Q. Ramasse, R. Zan, U. Bangert, D. W. Boukhvalov, Y.-W. Son and K. S. Novoselov, *ACS Nano*, 2012, **6**, 4063–4071.
- X. Li, W. Cai, J. An, S. Kim, J. Nah, D. Yang, R. Piner, A. Velamakanni, I. Jung, E. Tutuc, S. K. Banerjee, L. Colombo and R. S. Ruoff, *Science*, 2009, **324**, 1312–1314.
- Q. Yu, L. a Jauregui, W. Wu, R. Colby, J. Tian, Z. Su, H. Cao, Z. Liu, D. Pandey, D. Wei, T. F. Chung, P. Peng, N. P. Guisinger, E. a Stach, J. Bao, S.-S. Pei and Y. P. Chen, *Nat. Mater.*, 2011, **10**, 443–449.
- C. Mattevi, H. Kim and M. Chhowalla, *J. Mater. Chem.*, 2011, **21**, 3324–3334.
- S. Malola, H. Häkkinen and P. Koskinen, *Appl. Phys. Lett.*, 2009, **94**, 043106.
- O. V. Yazyev and A. Pasquarello, *Phys. Rev. B*, 2010, **82**, 045407.
- O. Lehtinen, N. Vats, G. Algara-siller, P. Knyrim and U. Kaiser, *Nano Lett.*, 2015, **15**, 235–241.
- J. H. Warner, E. R. Margine, M. Mukai, A. W. Robertson, F. Giustino and A. I. Kirkland, *Science*, 2012, **337**, 209–212.
- J. Ma, D. Alfè, A. Michaelides and E. Wang, *Phys. Rev. B*, 2009, **80**, 033407.
- L. Li, S. Reich and J. Robertson, *Phys. Rev. B*, 2005, **72**, 184109.
- W. Zhang, L. Sun, Z. Xu, A. V. Krasheninnikov, P. Huai, Z. Zhu and F. Banhart, *Phys. Rev. B*, 2010, **81**, 125425.
- J. Lee, W. Zhou, S. J. Pennycook, J.-C. Idrobo and S. T. Pantelides, *Nat. Commun.*, 2013, **4**, 1650.
- P. Koskinen, S. Malola and H. Häkkinen, *Phys. Rev. Lett.*, 2008, **101**, 115502.
- L. Reimer and H. Kohl, *Transmission Electron Microscopy*. Springer, USA, 2008.
- A. V. Krasheninnikov, F. Banhart, J. X. Li, a. S. Foster and R. M. Nieminen, *Phys. Rev. B*, 2005, **72**, 125428.
- A. Zobelli, A. Gloter, C. P. Ewels, G. Seifert and C. Colliex, *Phys. Rev. B*, 2007, **75**, 245402.
- Y. Gan, L. Sun and F. Banhart, *Small*, 2008, **4**, 587–591.
- D. W. Boukhvalov and M. I. Katsnelson, *Appl. Phys. Lett.*, 2009, **95**, 023109.
- E. Kano, M. Takeguchi, J. Fujita and A. Hashimoto, *Carbon*, 2014, **80**, 382–386.
- Y. Hao, M. S. Bharathi, L. Wang, Y. Liu, H. Chen, S. Nie, X. Wang, H. Chou, C. Tan, B. Fallahzad, H. Ramanarayan, C. W. Magnuson, E. Tutuc, B. I. Yakobson, K. F. McCarty, Y.-W. Zhang, P. Kim, J. Hone, L. Colombo and R. S. Ruoff, *Science*, 2013, **342**, 720–723.
- <https://azuma.nims.go.jp/>
- J. P. Perdew, K. Burke and M. Ernzerhof, *Phys. Rev. Lett.*, 1996, **77**, 3865–3868.
- D. Vanderbilt, *Phys. Rev. B*, 1990, **41**, 7892–7895.
- H. J. Monkhorst and J. D. Pack, *Phys. Rev. B*, 1976, **13**, 5188–5191.
- G. Henkelman, B. P. Uberuaga and H. Jónsson, *J. Chem. Phys.*, 2000, **113**, 9901–9904.